

## Article

# Joint Estimation of SOC and SOH for Lithium-Ion Batteries Based on Dual Adaptive Central Difference H-Infinity Filter

Bingyu Sang <sup>1,2,\*</sup>, Zaijun Wu <sup>1</sup>, Bo Yang <sup>2</sup>, Junjie Wei <sup>3</sup> and Youhong Wan <sup>3</sup><sup>1</sup> School of Electrical Engineering, Southeast University, Nanjing 211189, China; zjwu@seu.edu.cn<sup>2</sup> China Electric Power Research Institute, Nanjing 210003, China; yb\_11122@163.com<sup>3</sup> College of Automation & College of Artificial Intelligence, Nanjing University of Posts and Telecommunications, Nanjing 210023, China; 1222056203@njupt.edu.cn (J.W.); wanyh@njupt.edu.cn (Y.W.)

\* Correspondence: bys\_24@163.com

**Abstract:** The accurate estimation of the state-of-charge (SOC) and state-of-health (SOH) of lithium-ion batteries is crucial for the safe and reliable operation of battery systems. In order to overcome the practical problems of low accuracy, slow convergence and insufficient robustness in the existing joint estimation algorithms of SOC and SOH, a Dual Adaptive Central Difference H-Infinity Filter algorithm is proposed. Firstly, the Forgetting Factor Recursive Least Squares (FFRLS) algorithm is employed for parameter identification, and an inner loop with multiple updates of the parameter estimation vector is added to improve the accuracy of parameter identification. Secondly, the capacity is selected as the characterization of SOH, and the open circuit voltage and capacity are used as the state variables for capacity estimation to improve its convergence speed. Meanwhile, considering the interaction between SOC and SOH, the state space equations of SOC and SOH estimation are established. Moreover, the proposed algorithm introduces a robust discrete H-infinity filter equation to improve the measurement update on the basis of the central differential Kalman filter with good accuracy, and combines the Sage-Husa adaptive filter to achieve the joint estimation of SOC and SOH. Finally, under Urban Dynamometer Driving Schedule (UDDS) and Highway Fuel Economy Test (HWFET) conditions, the SOC estimation errors are 0.5% and 0.63%, and the SOH maximum estimation errors are 0.73% and 0.86%, indicating that the proposed algorithm has higher accuracy compared to the traditional algorithm. The experimental results at different initial values of capacity and SOC demonstrate that the proposed algorithm showcases enhanced convergence speed and robustness.

**Keywords:** joint estimation of SOC and SOH; improved forgetting factor least squares; dual adaptive center difference H $\infty$  filter



**Citation:** Sang, B.; Wu, Z.; Yang, B.; Wei, J.; Wan, Y. Joint Estimation of SOC and SOH for Lithium-Ion Batteries Based on Dual Adaptive Central Difference H-Infinity Filter. *Energies* **2024**, *17*, 1640. <https://doi.org/10.3390/en17071640>

Academic Editor: Abdul-Ghani Olabi

Received: 8 March 2024

Revised: 24 March 2024

Accepted: 26 March 2024

Published: 29 March 2024



**Copyright:** © 2024 by the authors. Licensee MDPI, Basel, Switzerland. This article is an open access article distributed under the terms and conditions of the Creative Commons Attribution (CC BY) license (<https://creativecommons.org/licenses/by/4.0/>).

## 1. Introduction

Lithium-ion batteries are extensively utilized in electric vehicles and energy storage systems due to their advantageous features, including long cycle life, high energy density, and low self-discharge rate [1]. SOC and SOH are two important parameters in the battery management system (BMS) [2], which provide important references for battery safety protection, charge/discharge control, etc. Therefore, it is important to obtain the SOC and SOH information accurately and in a timely manner to improve battery life and safety.

SOC can be predicted directly by the Coulomb counting method [3] and the open-circuit voltage method [4]. However, the former method is significantly influenced by initial SOC discrepancies, while sensor measurement inaccuracies further diminish SOC estimation accuracy over time. The open-circuit voltage method requires the battery to rest for a sufficient duration before estimating the SOC, rendering it unsuitable for real-time estimation applications. Machine learning-based methods such as artificial neural networks [5], deep neural networks [6], and Gaussian process regression [7] have also found applications in SOC estimation, but these approaches require large and comprehensive training data, and the results are susceptible to different datasets. In addition, there

are the Kalman filter (KF) and its derivative algorithms, including the extended Kalman filter (EKF) [8], CDKF [9], H-infinity filter [10], adaptive Kalman filter [11,12] and other algorithms. The KF can better resist noise interference and has low dependence on the initial value [13], so the KF is recognized as the most widely employed method in SOC estimation.

At present, a single SOC estimation method ignores the capacity degradation under the influence of battery aging, which could result in considerable errors in SOC estimation. Therefore, the joint estimation of SOC and SOH is highly necessary. Shen et al. [14] calculated the capacity by the ratio of the accumulated charge to the SOC change value over a period of time. This is an offline estimation method, while the accuracy of the capacity estimation is affected by the magnitude of the SOC change value over that period of time. Zou et al. [15] placed the capacity and SOC within the same state vector and achieved the joint estimation of SOC and SOH using a fourth-order EKF. Because SOC and capacity are not decoupled, the convergence of capacity estimation tend to be slow. Lai et al. [16] proposed a data-driven method based on the NSSR-LSTM Neural Network to achieve the joint estimation of SOC and SOH for lithium-ion batteries. However, their generalization to untrained cases is usually weak. Since the actual battery configuration file usually has great uncertainty, a large amount of training data is needed to meet the accuracy of joint estimation in different scenarios. To address the above problems, numerous researchers have proposed a dual filter algorithm to estimate the SOC and capacity of the battery separately. Cheng et al. [17] proposed a joint estimation algorithm of adaptive square root unscented Kalman filter (ASRUKF) and EKF, where the ohmic resistance and capacity parameters are estimated by EKF and brought into SOC estimation. At the same time, the SOC value estimated by ASRUKF is used to update these two parameters in real-time. Liu et al. [18] proposed a dual adaptive extended particle filter (DAEPF) to estimate the SOC and SOH of the battery. The algorithm combines the advantages of EKF and particle filter (PF) so that the algorithm not only has accurate initial state estimation and covariance information but also can adapt to nonlinear systems and non-Gaussian noise. However, due to the insufficient accuracy of the EKF and the high computational complexity of the PF, this fusion algorithm cannot accurately estimate the SOC and SOH information of the battery, and the computational cost is high. The dual adaptive unscented Kalman filter (DAUKF) is proposed in the literature [19]. The battery parameters and SOC are updated through two AUKF filters, respectively, which have certain estimation accuracy and stability. Since the open circuit voltage (OCV) has a certain relationship with SOC and capacity, OCV is crucial for accurately obtaining SOC values as well as for accurate and timely capacity estimation. These joint estimation algorithms do not consider the close relationship between OCV and capacity. Therefore, the accuracy and convergence speed of capacity estimation are difficult to guarantee under inaccurate OCV estimation. Yu et al. [20] proposed a joint estimation algorithm of RLS and adaptive H-infinity filter to realize online capacity estimation, which reduces the influence of OCV on capacity estimation. However, the AHIF algorithm used has the problem of high-order accuracy loss caused by the simple linearization of nonlinear functions, so the accuracy of the algorithm is limited, and it is difficult to ensure the accuracy of OCV and capacity estimation.

In view of the above problems, this paper uses an improved FFRLS (IFFRLS) algorithm based on the 2RC equivalent circuit model to improve the accuracy of parameter identification. Then, the CDKF algorithm with higher accuracy is used to fuse the H-infinity filter equations in the measurement update stage, and the ACDHF algorithm is obtained by combining the Sage–Husa adaptive filter. Since this algorithm combines both the accuracy of the CDKF and the robustness of the H-infinity filter, the DACDHF algorithm proposed in this paper has higher estimation accuracy and better robustness compared to the traditional algorithms, and also avoids the complex operation of solving the Jacobi matrix of the system matrix in the literature [20]. In addition, the capacity is selected as the index of SOH, and the close connection between capacity and OCV is considered to realize the SOH estimation with capacity and OCV as state variables. In the case of accurate OCV estimation results, the influence of OCV on capacity estimation accuracy and convergence speed is weakened,

and thus, the capacity estimation method in this paper has a faster convergence speed compared to the traditional capacity estimation method. Finally, two ACDHF filters are used to estimate SOC and capacity, respectively, and the proposed algorithm is verified to have better estimation accuracy, robustness, and convergence speed under several typical working conditions.

The subsequent sections of this paper are organized as follows: Section 2 introduces battery modeling and parameter identification. In Section 3, the SOC-SOH joint estimation method is presented. Analysis of the results is provided in Section 4, followed by the conclusions in Section 5.

## 2. Battery Modeling and Parameter Identification

### 2.1. Battery Modeling

The two-RC equivalent circuit model is used, and the circuit diagram is shown in Figure 1, where  $U_{oc}$  is the OCV;  $U_t$  is the terminal voltage;  $R_p$  and  $C_p$  are the electrochemical polarization resistance and capacitance;  $R_d$  and  $C_d$  are the concentration polarization resistance and capacitance;  $R_o$  is the ohmic resistance;  $I$  is the battery current, where charging is positive; and  $U_p$  and  $U_p$  are the terminal voltage of the two-RC circuit.

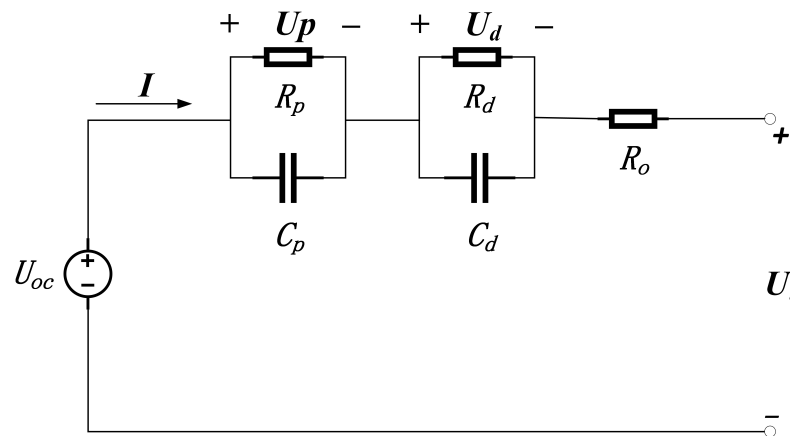


Figure 1. Battery model.

The modeling equations of the battery are as follows:

$$\begin{cases} \dot{U}_p = -\frac{1}{R_p C_p} U_p + \frac{1}{C_p} I \\ \dot{U}_d = -\frac{1}{R_d C_d} U_d + \frac{1}{C_d} I \\ U_t = U_{oc} - U_p - U_d - IR_o \end{cases} \quad (1)$$

The SOC of the battery can be calculated by the Coulomb counting method:

$$SOC_k = SOC_0 - \frac{\eta}{Q_c} \int_0^k I_k dk \quad (2)$$

where  $SOC_0$  is the SOC at the initial moment;  $Q_c$  is the calibrated capacity of the battery;  $I_k$  is the current at the  $k$  moment; and  $\eta$  is the Coulomb coefficient.

From Equations (1) and (2), the state space equation for battery SOC estimation is obtained as follows:

$$x_k = \begin{bmatrix} e^{-\frac{\Delta t}{\tau_p}} & 0 & 0 \\ 0 & e^{-\frac{\Delta t}{\tau_d}} & 0 \\ 0 & 0 & 1 \end{bmatrix} x_{k-1} + \begin{bmatrix} R_p(1 - e^{-\frac{\Delta t}{\tau_p}}) \\ R_d(1 - e^{-\frac{\Delta t}{\tau_d}}) \\ \Delta t \times \frac{\eta}{Q_{c,k}} \end{bmatrix} \times I_{k-1} + \omega_k \quad (3)$$

$$U_{t,k} = f(SOC_k) - U_{p,k} - U_{d,k} - R_o \times I_k + v_k \quad (4)$$

where  $x_k = [U_{p,k} \ U_{d,k} \ SOC_k]^T$  is the state vector;  $\omega_k$  and  $v_k$  are the process noise and measurement noise, respectively;  $\tau_p = R_p C_p, \tau_d = R_d C_d; \Delta t$  is the sampling time;  $f()$  is a function of  $U_{oc}$  on SOC, which can be fitted by the correspondence between SOC and  $U_{oc}$ ; and  $Q_{c,k}$  is the updated result of the capacity estimation, which is brought into the SOC estimation in real-time.

2.2. The Relationship between the State-of-Charge and Open-Circuit Voltage

In this paper, we examine the NCR18650PF power lithium battery produced by Panasonic, which features a nominal voltage of 3.6 V and a rated capacity of 2.9 Ah. The data sampling frequency is 10 Hz, and the experiment is carried out at 25 °C. To obtain a more precise SOC-OCV curve, this paper adopts the static voltage method [21] for the experiment, and the sampling points taken are shown in Table 1:

Table 1. SOC-OCV relationship table.

SOC/%	100	90	80	70	60
OCV/V	4.175	4.059	3.947	3.862	3.768
50	40	30	20	10	5
3.663	3.602	3.55	3.458	3.345	3.237

To prevent overfitting as well as to consider the amount of computation, a 6th-order fitting method is used. The fitting curve is depicted in Figure 2, and the SOC-OCV relationship equation is as follows:

$$U_{oc} = 3.4290 \times SOC^6 - 4.4888 \times SOC^5 - 6.3228 \times SOC^4 + 14.9681 \times SOC^3 - 9.7608 \times SOC^2 + 3.2527 \times SOC + 3.0984 \tag{5}$$

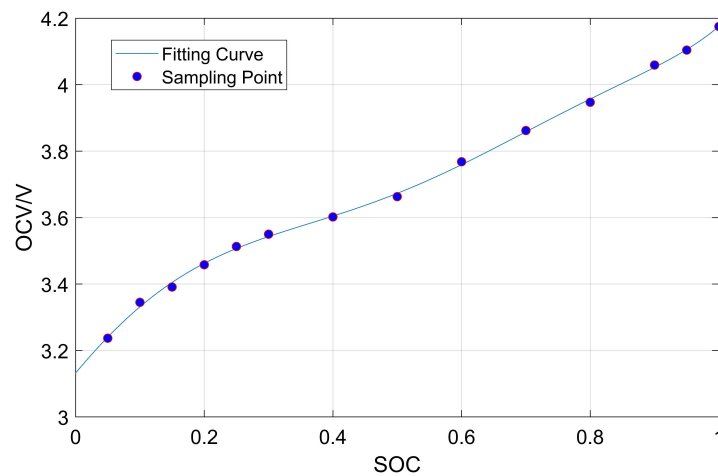


Figure 2. SOC-OCV relationship curve.

2.3. Improved FFRLS

In this paper, the FFRLS algorithm is used to identify the parameters of lithium-ion battery model. The algorithm can achieve online parameter identification by the recursive least squares method, and can solve the data saturation in the recursive least squares algorithm by introducing the forgetting factor. It usually takes the value of 0.90–1.00, and the value of the forgetting factor selected in this paper is 0.998. The FFRLS expressions are as follows:

$$\begin{cases} \hat{\theta}_k = \hat{\theta}_{k-1} + K_k [U_k - \varphi_k^T \hat{\theta}_{k-1}] \\ K_k = H_{k-1} \varphi_k [\varphi_k^T H_{k-1} \varphi_k + \lambda]^{-1} \\ H_k = \frac{1}{\lambda} [E - K_k \varphi_k^T] H_{k-1} \end{cases} \tag{6}$$

where  $\hat{\theta}_k$  is the estimated parameter vector;  $U_k$  is the system input value;  $K_k$  is the gain matrix;  $\varphi_k$  is the data vector;  $H_k$  is the error covariance matrix; and  $E$  is the unit matrix.

Adding an inner loop with multiple updates of the parameter estimation vectors to the traditional FFRLS algorithm can improve the accuracy of model parameter identification [22], thus further improving the accuracy of the joint estimation. Let  $M$  be the number of iterations of the inner loop, then the initial inner loop estimation vector is  $\hat{\theta}_{in,0} = \hat{\theta}_{k-1}$ , and the parameter estimation update step of the inner loop is as follows:

$$\hat{\theta}_{m,m} = \hat{\theta}_{m,m-1} + K_k [U_k - \varphi_k^T \hat{\theta}_{m,m-1}], 1 \leq m = m + 1 \leq M \tag{7}$$

#### 2.4. Model Parameter Identification

The impulse transfer function of the lithium battery model is obtained from Equation (1):

$$G(z) = \frac{a_3 + a_4z^{-1} + a_5z^{-2}}{1 - a_1z^{-1} - a_2z^{-2}} \tag{8}$$

Let  $U_k = U_{t,k} - U_{oc,k}$  transform Equation (8) into the form of a difference equation:

$$U_k = a_1U_{k-1} + a_2U_{k-2} + a_3I_k + a_4I_{k-1} + a_5I_{k-2} \tag{9}$$

where  $a_1 - a_5$  is the parameter to be recognized.

Let  $\varphi_k = [U_{k-1}, U_{k-2}, I_k, I_{k-1}, I_{k-2}]^T$ ,  $\hat{\theta} = [a_1, a_2, a_3, a_4, a_5]$ . Let  $\hat{\theta}_0, \hat{\theta}_1$  be a reasonable initial value,  $P_0$  be  $10^5 \times E_{5 \times 5}$ , and  $E_{5 \times 5}$  be a 5th order unit matrix. Using the UDDS conditions data, the IFFRLS is applied for parameter identification to obtain each resistance and capacitance value of the model. Figure 3 illustrates the voltage simulation values and the actual voltage values estimated by both the traditional FFRLS and the FFRLS with different inner loops.

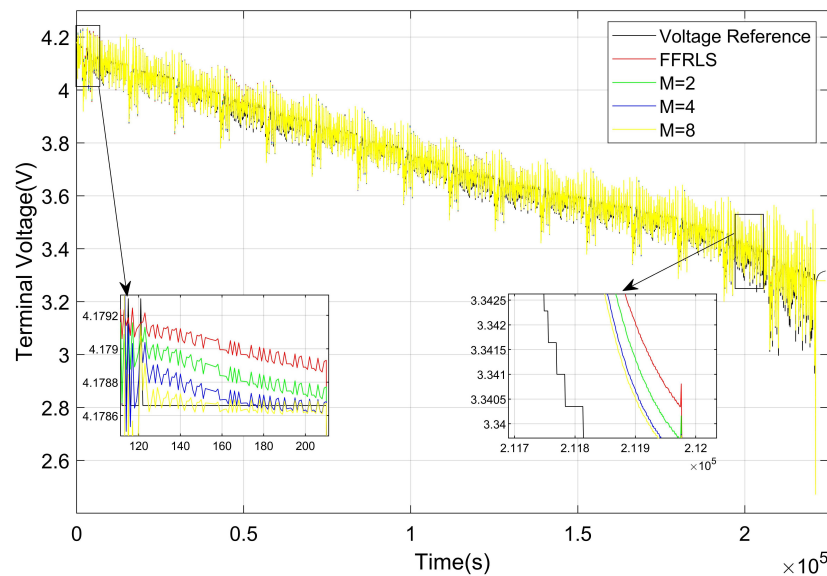


Figure 3. Model output and actual voltage.

Table 2 shows the performance index and runtime comparison information of conventional FFRLS and IFFRLS for identifying battery parameters. It can be seen that the IFFRLS algorithm has stronger tracking ability and better recognition accuracy, and the error of the identification algorithm decreases with the increase in the number of inner loops. Among them, compared with the FFRLS, when the number of inner loops  $M = 2$ , the accuracy improvement is more obvious. When  $M = 4$  and  $M = 8$ , the accuracy improvement of the algorithm is limited, and the time cost of the algorithm operation increases obviously. For comprehensive consideration, the parameter identification result of  $M = 2$  is selected in this paper.

**Table 2.** Performance metrics of FFRLS with different numbers of inner loop.

	MRE (%)	MAE (V)	RMSE (V)	t/s
FFRLS (M = 0)	0.26023	0.0093640	0.013023	1.74
M = 2	0.24618	0.0088864	0.011873	1.79
M = 4	0.23972	0.0086771	0.011361	1.96
M = 8	0.23855	0.0086541	0.011293	2.23

### 3. Joint Estimation of SOC and SOH Based on DACDHF

#### 3.1. Joint Estimation of SOC and SOH

In order to address the issue of capacity degradation under the influence of ignoring battery aging in the single SOC estimation algorithm, this paper uses the DACDHF algorithm for joint estimation, and the flowchart is illustrated in Figure 4. At present, the conventional joint estimation methods tend to overlook the intimate connection between OCV and capacity. However, in the case of inaccurate OCV estimation, the accuracy and convergence speed of capacity estimation will be affected. To solve the problem, on the one hand, the capacity estimator is designed based on the relationship between OCV and capacity, and the SOC is updated using the estimated capacity results. On the other hand,  $\chi = dU_{oc}/dSOC$  is introduced into the capacity estimation to reveal the effect of SOC on capacity estimation.

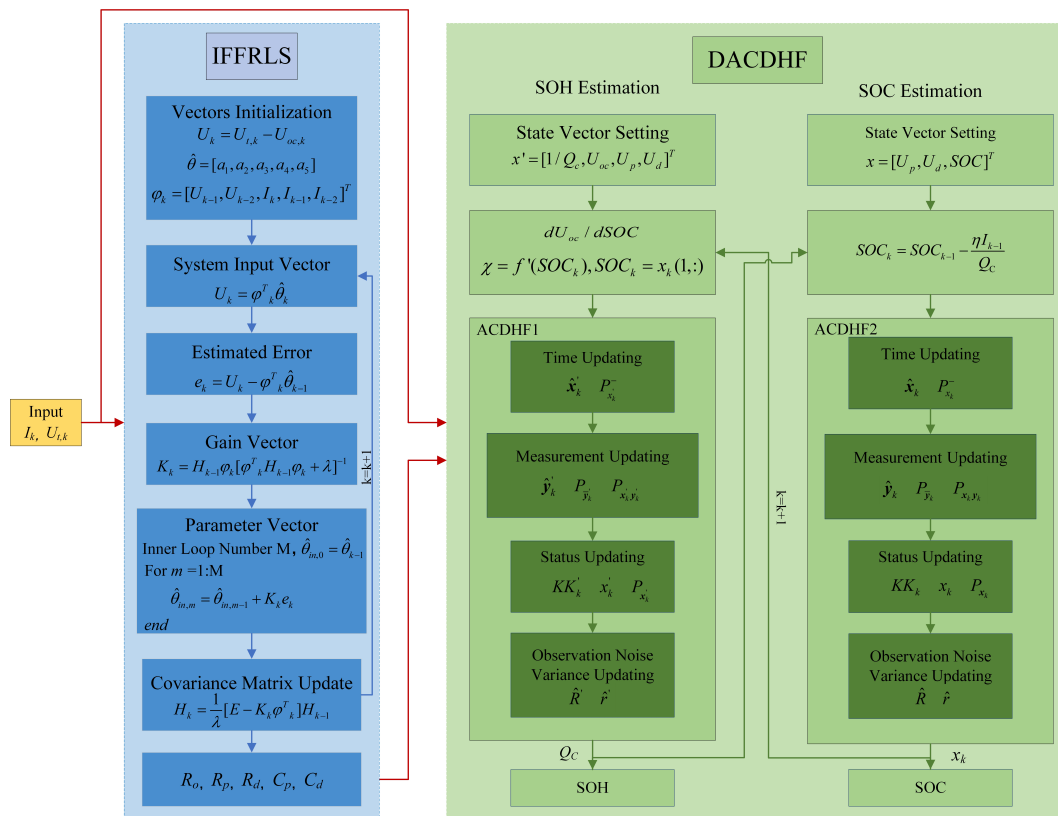


**Figure 4.** Joint estimation flowchart.

SOH is a crucial indicator used to evaluate the extent of battery aging or deterioration. The chemical reactions and physical processes inside the battery inevitably lead to battery decline, resulting in a decrease in SOH over the battery’s lifespan. In this study, the capacity is selected as the characterization of SOH, and the SOH calculation formula is:

$$SOH = \frac{Q_c}{Q_N} \times 100\% \tag{10}$$

where  $Q_c$  and  $Q_N$  are the current maximum usable capacity and rated capacity of the battery, respectively. It is generally recognized that when the maximum available capacity of the battery is reduced to 80% of the rated capacity (i.e., SOH = 80%), the battery life is terminated and needs to be replaced.

In traditional parameter estimation research, when the battery discharges at a low current or the sampling time is sufficiently short, it is usually considered that the OCV between adjacent sampling points do not change, i.e.,  $dU_{oc}/dt = 0$ , then  $U_{oc,k} = U_{oc,k-1}$ . However, in the actual dynamic test conditions, where batteries do not always discharge at small currents or the sampling time is not always short enough, it is not reasonable to assume that the OCV remains unchanged at adjacent sampling points [20]. In this paper, we consider that the OCV between adjacent sampling points is changing, i.e.,  $\frac{dU_{oc}}{dt} = \frac{dU_{oc}}{dSOC} \cdot \frac{dSOC}{dt}$ . Combined with Equation (2), the relationship between the OCV and capacity can be obtained as Equation (11):

$$U_{oc,k} = U_{oc,k-1} - \chi_{k-1} \frac{\eta I_{k-1} \Delta t}{Q_c} \quad (11)$$

where  $\frac{dU_{oc}}{dt} = \frac{dU_{oc}}{dSOC} \cdot \frac{dSOC}{dt}$ , it can be calculated by deriving the function SOC-OCV in Equation (5).

In the case of Li-ion batteries, the capacity can be considered constant during the single charge/discharge cycle. When the capacity  $Q_c$  is directly selected as the state, the  $\gamma$  of ACDHF algorithm never satisfies the lower bound condition for the normal operation of the algorithm (it is given by Equation (19)), so the inverse of the capacity  $1/Q_c$  is selected as the state. Since the accuracy of the OCV estimation may have an effect on the convergence speed of the capacity estimation, the OCV is simultaneously selected as one of the capacity estimation states in this paper. The OCV is estimated by the algorithm proposed in this paper, and its effect on the convergence speed of capacity estimation is weakened when the OCV estimation is accurate, i.e., the state vector of the capacity estimation is set to  $x'_k = [1/Q_{c,k} \ U_{oc,k} \ U_{p,k} \ U_{d,k}]^T$ . Combining Equations (1) and (11), the state space equations for battery capacity estimation are:

$$x'_k = Ax'_{k-1} + BI_{k-1} + \omega'_k \quad (12)$$

$$U_{t,k} = U_{oc,k} - U_{p,k} - U_{d,k} - I_k R_o + v'_k \quad (13)$$

where  $\omega'_k$  and  $v'_k$  are the process noise and the measurement noise of the capacity estimation at moment  $k$  of the capacity estimation, respectively. The state space matrix is:

$$A = \begin{bmatrix} 1 & 0 & 0 & 0 \\ -\chi_{k-1} \eta I_{k-1} \Delta t & 1 & 0 & 0 \\ 0 & 0 & e^{-\Delta t / \tau_p} & 0 \\ 0 & 0 & 0 & e^{-\Delta t / \tau_d} \end{bmatrix}, B = \begin{bmatrix} 0 \\ 0 \\ (1 - e^{-\Delta t / \tau_p}) R_p \\ (1 - e^{-\Delta t / \tau_d}) R_d \end{bmatrix} \quad (14)$$

### 3.2. Adaptive Center Difference $H_\infty$ Filtering (ACDHF) Algorithm

CDKF overcomes the high-order accuracy loss caused by first-order linearization, and has higher accuracy than the EKF algorithm. However, due to the limitation of the KF framework, its robustness is not as good as the H-infinity filter. CDHF mainly introduces a robust H-infinity filter to improve the posterior covariance matrix in the CDKF measurement update step. The improved covariance matrix is as follows (taking SOC estimation parameters as an example):

$$P_{x_k} = P_{x_k}^- - \begin{bmatrix} P_{x_k y_k} & P_{x_k}^- \end{bmatrix} \begin{bmatrix} P_{y_k}^- & P_{x_k y_k}^T \\ P_{x_k y_k}^- & P_{x_k}^- - \gamma E \end{bmatrix} \begin{bmatrix} P_{x_k y_k}^- \\ (P_{x_k}^-)^T \end{bmatrix} \quad (15)$$

where  $P_{x_k}$  is the covariance matrix of the system state;  $\gamma$  is defined to limit the maximum estimation error;  $P_{x_k y_k}$  and  $P_{\bar{y}_k}$  are the mutual covariance matrix and covariance matrix of the systematic observation; and  $E$  is the unit matrix.

In addition, the time update steps of CDHF and CDKF are exactly the same, so the posterior covariance matrix should satisfy the positive definite condition; otherwise, the algorithm cannot work properly. It is difficult to determine the positive definite condition directly for Equation (15), so it is obtained by using matrix inverse lemma transformation:

$$(P_{x_k})^{-1} = (P_{x_k}^-)^{-1} + V_k N_k V_k^T - \frac{1}{\gamma} E \tag{16}$$

$$V_k = (P_{x_k}^-)^{-1} P_{x_k y_k} \tag{17}$$

$$N_k = [P_{y_k} - P_{x_k y_k}^T (P_{x_k}^-)^{-1} P_{x_k y_k}]^{-1} \tag{18}$$

If  $P_{x_k}$  is to be positively determined, then it must be satisfied:

$$\gamma > \max \{ \text{eig}((P_k)^{-1} + V_k N_k V_k^{-1}) \} \tag{19}$$

where  $\max \{ \text{eig}()^{-1} \}$  represents the maximum eigenvalue after matrix inversion. To ensure the proper functioning of the CDHF, the value of  $\gamma$  cannot be excessively small.

In order to reduce the interference of measurement noise, this paper introduces the Sage–Husa adaptive algorithm to dynamically estimate the statistical characteristics of measurement noise in real-time by utilizing the data of measurement variables in the filtering process. In this paper, the process noise covariance array  $Q$  is set to a constant value, while only the measurement noise covariance matrix  $R$  is updated in real-time. The updated formulas of the Sage–Husa adaptive algorithm are as follows:

$$d_k = \frac{1 - b}{1 - b^{k+1}}, 0 < b < 1 \tag{20}$$

$$\hat{r}_k = (1 - d_k) \hat{r}_{k-1} + d_k (y_k - \sum_{i=0}^{2L} \omega_i^{(m)} y_{i,k|k-1}) \tag{21}$$

$$\hat{R}_k = (1 - d_k) \hat{R}_{k-1} + d_k (e_k e_k^T - \sum_{i=1}^l [\omega_i^{(c)} (y_{i,k|k-1} - y_{L+i,k|k-1})^2 + \omega_i^{(c_2)} (y_{i,k|k-1} + y_{L+i,k|k-1} - 2y_{0,k|k-1})^2]) \tag{22}$$

where  $b$  is the forgetting factor,  $d_k$  is the weighting factor,  $\hat{r}_k$  is the bias estimation of the measurement noise,  $\hat{R}_k$  is the estimation of the measurement noise covariance matrix  $R$ ,  $L$  is the dimension of the state vector ( $L = 3$  for SOC estimation and  $L = 4$  for capacity estimation),  $e$  is new interest, and  $y_{i,k|k-1}$  is the predicted value of the measurement update.

Therefore, the system measurement update estimates  $\hat{y}_k^-$  in the CDHF measurement update phase and the update equation  $P_{\bar{y}_k}$  are as follows:

$$\hat{y}_k^- = \sum_0^{2L} \omega_i^{(m)} y_{i,k|k-1} + \hat{r}_k \tag{23}$$

$$P_{\bar{y}_k} = \sum_{i=1}^L [\omega_i^{(c_1)} (y_{i,k|k-1} - y_{L+i,k|k-1})^2 + \omega_i^{(c_2)} (y_{i,k|k-1} + y_{L+i,k|k-1} - 2y_{0,k|k-1})^2] + \hat{R}_k \tag{24}$$

where  $\omega_i^{(m)}, \omega_i^{(c_2)}, \omega_i^{(c_1)}$  is the weight corresponding to the sigma point.

#### 4. Experimental Verifications and Discussions

The experimental data of UDDS and HWFET are used to verify the SOC and SOH joint estimation algorithm proposed in this paper. At the same time, the influence of the IFFRLS parameter identification results on the accuracy of the joint estimation algorithm is verified, and the proposed algorithm is compared with the traditional DACDKF algorithm. The initial value of SOC is set to 0.6, and the initial values of capacity and open-circuit voltage are set to 1/2.9 and 4.175, respectively.

Under the UDDS condition, Figure 5 displays the capacity and its error estimation results, Figure 6 shows the OCV and its error estimation results, and the SOH estimation results are shown in Figure 7. In Figure 5a, the pink and black lines are the battery-rated capacity and actual capacity reference lines, respectively. The red and green curves are the capacity curves estimated by the DACDHF and DACDKF joint estimation algorithms (parameters identified by the traditional FFRLS). The blue curve is the capacity curve obtained by the DACDHF using the parameters identified by IFFRLS (internal loop number  $M = 2$ ), which is DACDHF ( $M = 2$ ). It can be seen from Figure 5a that the capacity curve demonstrates rapid convergence to the actual capacity, which avoids the problem of larger SOC estimation errors due to untimely capacity updates. In Figure 5b, after the curve converges, the average absolute error of the capacity estimated by the DACDHF is 0.0066 Ah, the average absolute estimation error of the capacity estimated by the DACDKF is 0.009 Ah, and the average absolute estimation error of the DACDHF ( $M = 2$ ) is 0.005 Ah. Therefore, compared with the DACDKF, the DACDHF in this paper has higher estimation accuracy. In addition, compared with the traditional FFRLS method, the data identified by the IFFRLS can further improve the estimation accuracy of the algorithm. In Figure 6, the blue curve is the DACDHF ( $M = 2$ ) estimation with a maximum estimation error of 5.5 mV, the red curve is the DACDHF estimation with a maximum estimation error of OCV less than 8 mV, and the green curve is the DACDKF estimation with a maximum error of less than 12 mV. The estimated value of OCV is more accurate, which also proves that the OCV estimated by the algorithm in this paper has little effect on the accuracy and convergence speed of capacity estimation. From the SOH curve in Figure 7, it is observable that the batteries in this group exhibit more pronounced aging, with the SOH of the batteries declining to about 0.93.

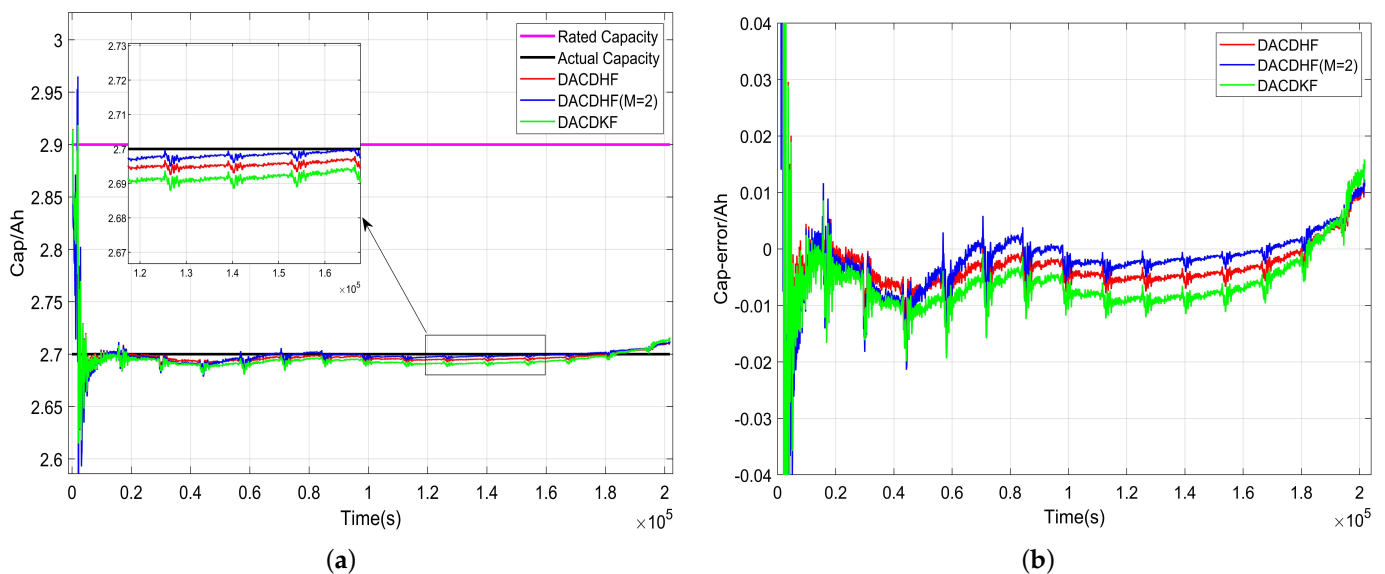


**Figure 5.** OCV and its error estimation results for UDDS conditions: (a) OCV estimation curve; (b) OCV estimation error curve.

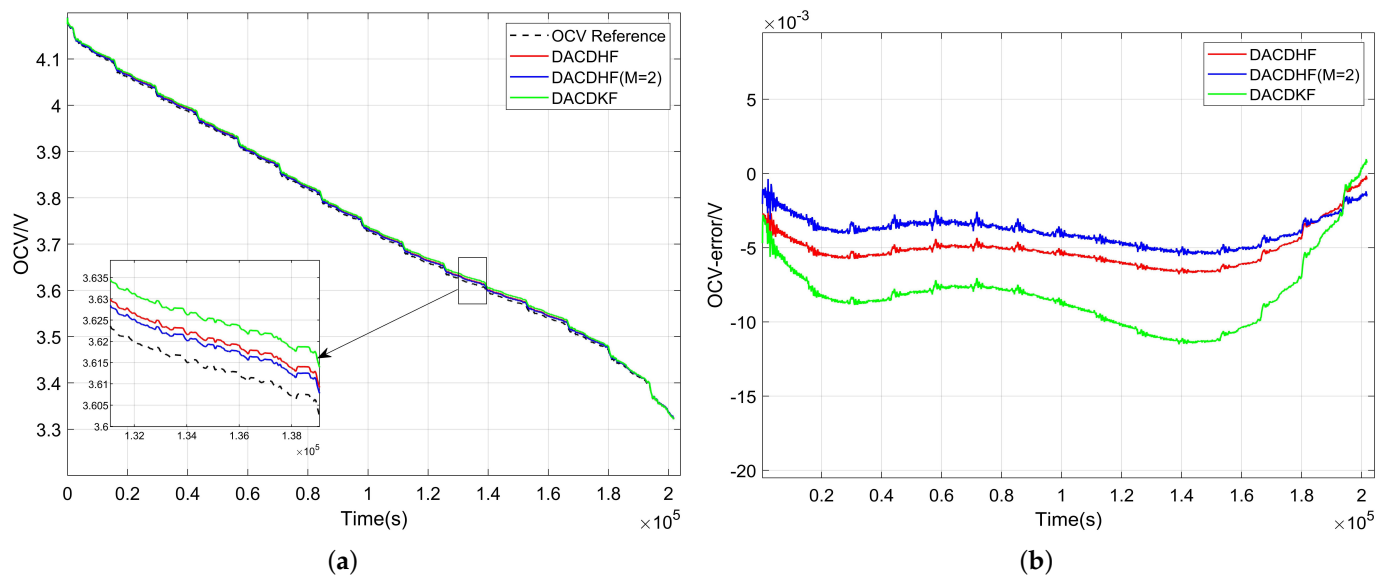


**Figure 6.** Capacity and its error estimation results for UDDS conditions: (a) capacity estimation curve; (b) capacity estimation error curve.

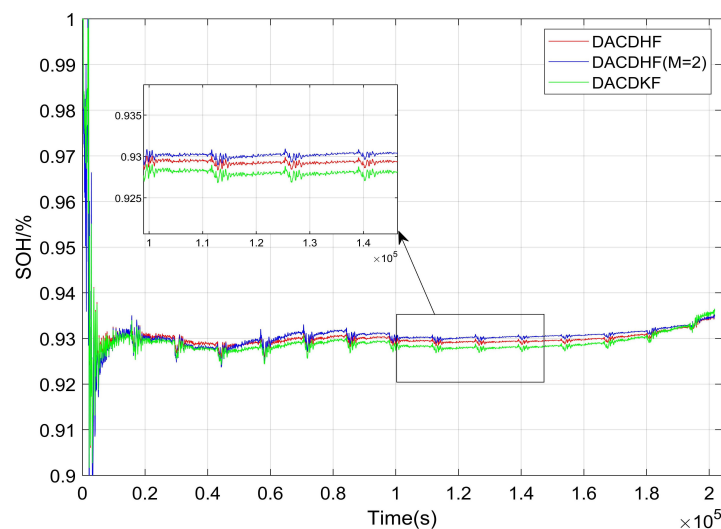


**Figure 7.** SOH estimation results for UDDS conditions.

In Figure 5a, the capacity curve can quickly converge to the actual capacity with a convergence time of less than 8 min. To validate the benefits of the proposed joint estimation algorithm in terms of convergence time, traditional joint estimation algorithms such as DEKF and multi-scale DEKF are used for comparison. The experimental results are presented in Table 3. It is observed that the traditional joint estimation method exhibits a notably slow convergence speed when there exists a deviation between the initial capacity value and the actual capacity. In contrast, the capacity estimation method proposed in this study demonstrates a faster convergence speed.

**Table 3.** Comparison of convergence times of different capacity estimation algorithms.

Estimation Algorithm	Initial Capacity Value	Convergence Time
DACDHF (M = 2)	2.9 Ah	<8 min
DEKF [23]	2.9 Ah	<140 min
Multiscale DEKF [23]	2.9 Ah	<140 min

The results of the capacity estimation are put into the SOC estimation in real-time, and the SOC and its error results are shown in Figure 8. In Figure 8a, the black curve is a single SOC estimation curve. It is evident that as the battery capacity declines, the single SOC estimation algorithm will experience significant deviation in the later stages. The joint estimation algorithm updates the results of the battery capacity estimation to the calculated value of the SOC estimation in real-time, which solves the problem that the single SOC estimation method ignores the battery capacity degradation under the influence of battery aging. From Figure 8b, it is observed that the maximum error of SOC estimation of the ACDHF algorithm without capacity update is 5.5%, while the average error of SOC estimation of the DACDKF joint estimation algorithm is 1.1%, the average error of SOC estimation of the DACDHF joint estimation algorithm is 0.58%, and the average error of SOC estimation of the DACDHF (M = 2) joint estimation algorithm is 0.50%. Therefore, the joint estimation algorithm has higher accuracy in SOC estimation.

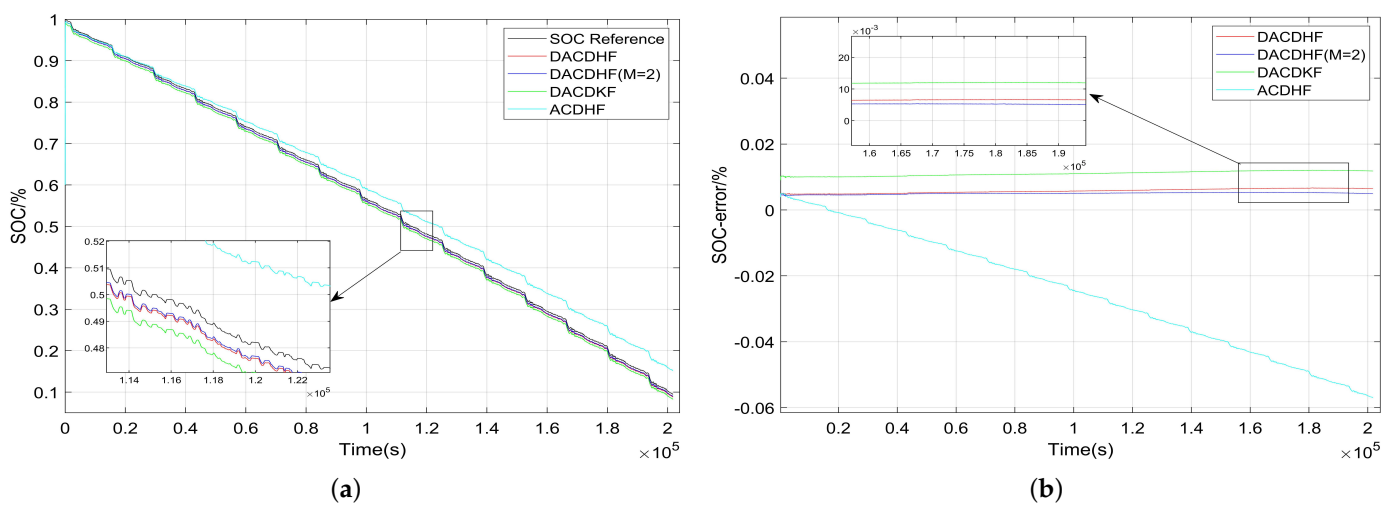


**Figure 8.** SOC estimation results and SOC error results for UDDS conditions: (a) SOC estimation results; (b) SOC error results.

The accuracy of capacity estimation, OCV estimation, and SOC estimation across three joint estimation algorithms: DACDKF, DACDHF, and DACDHF (M = 2) is shown in Table 4. The table employs absolute mean (MAE) and root mean square error (RMSE) metrics for evaluation. As shown in Table 4, the accuracy of the DACDHF algorithm in capacity estimation, OCV estimation, and SOC estimation is better than that of the DACDKF algorithm, and the parameters identified by the IFFRLS algorithm can further improve the estimation accuracy.

**Table 4.** Performance comparison of different joint estimation algorithms.

Estimation Algorithm	Capacity Estimation		OCV Estimation		SOC Estimation	
	MAE/%	RMSE/%	MAE/%	RMSE/%	MAE/%	RMSE/%
DACDKF	0.9	1.778	0.813	0.848	1.11	1.24
DACDHF	0.823	1.737	0.507	0.523	0.577	0.592
DACDHF (M = 2)	0.542	1.621	0.384	0.397	0.501	0.516

To verify the robustness of the algorithm, experiments are carried out with different initial values of capacity, OCV, and SOC. Firstly, the initial value of the capacity estimation state is set to  $x' = [1/3; 3.9; 0; 0]$ , and the initial SOC is set to 0.6. Figure 9 shows the capacity and OCV estimation results.

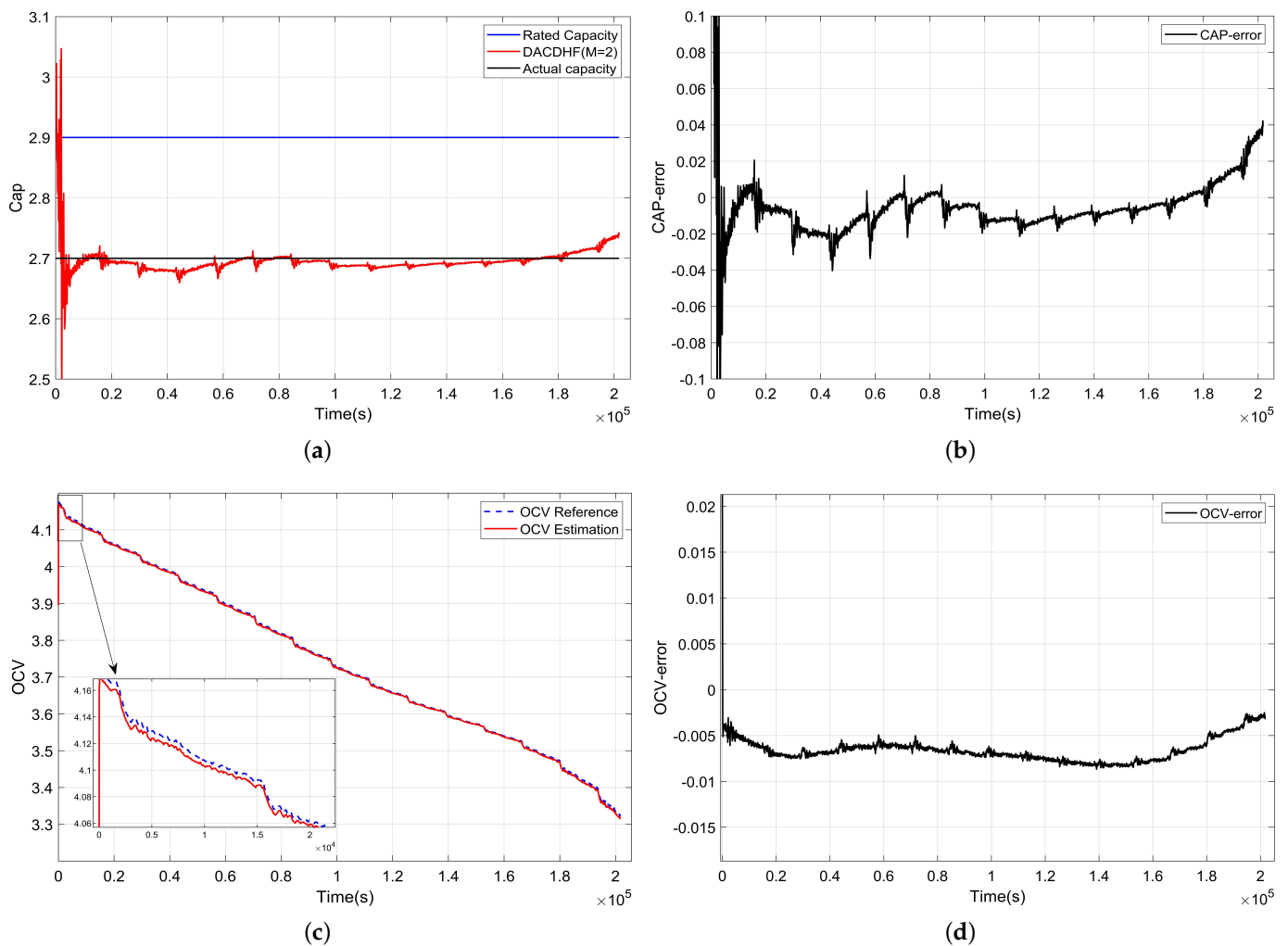


**Figure 9.** Capacity and OCV estimation results with initial value of  $x' = [1/3; 3.9; 0; 0]$ ; (a) capacity estimation curve; (b) capacity error curve; (c) OCV estimation curve; (d) OCV error curve.

The initial value of the capacity estimation is guaranteed to be  $x' = [1/3; 3.9; 0; 0]$ . Different SOC initial values are set to observe the estimation results of SOC. The initial values of SOC are set to 0.2, 0.4 and 0.6 respectively, and the SOC estimation and its error results are obtained as shown in Figure 10.

As shown in Figure 9, when the initial capacity value is set to 3 Ah and the OCV is set to 3.9 V, both the capacity estimation error and the OCV estimation error experience a slight increase. The maximum error in capacity estimation is 0.047 Ah, while the OCV converges rapidly to the reference value, with a maximum estimation error of less than 10 mV. In Figure 10, the initial value of the capacity estimation is constant. As the error of the initial value of SOC increases, the convergence time of the SOC estimation increases, and the maximum error increases from 0.78% to 0.96%. However, the overall errors remain within a small range, indicating the high estimation accuracy and robustness of the DACDHF algorithm. The initial SOC value is set to 0.6, and the estimation results under different initial values of capacity and OCV are presented in Table 5.

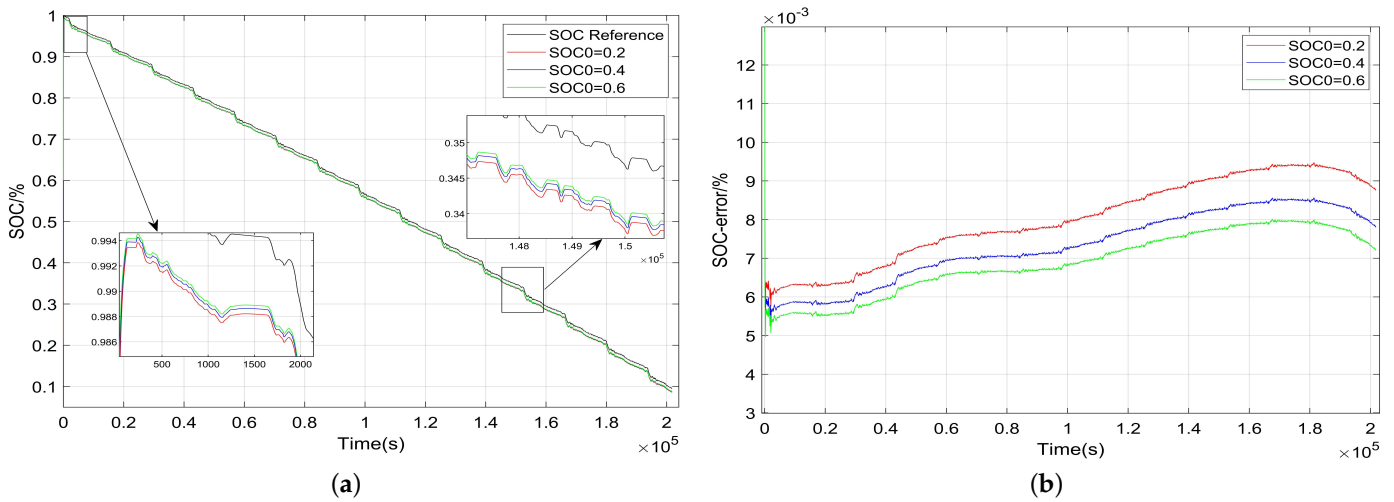


**Figure 10.** SOC estimation and error curves for different SOC initial values; (a) SOC estimation curve; (b) SOC error curve.

**Table 5.** Estimated results of capacity and OCV for different initial values.

Initial Capacity	Initial OCV	Capacity Estimation Error	OCV Estimation Error
3.1 Ah	3.9 V	0.089 Ah	15 mv
3.1 Ah	3.7 V	0.108 Ah	24 mv
3.2 Ah	3.7 V	0.14 Ah	29 mv

Figures 11–14 shows the capacity, OCV, and SOC estimation results under HWFET conditions. It can be seen that the OCV error of the battery is about 10 mv, which is more accurate. Capacity and SOC also have good estimation results under this complex current condition. The maximum estimation error of capacity is 0.025 Ah, and the maximum estimation error of SOC is 0.63%, which reflects the superiority of the joint estimation algorithm in this paper.

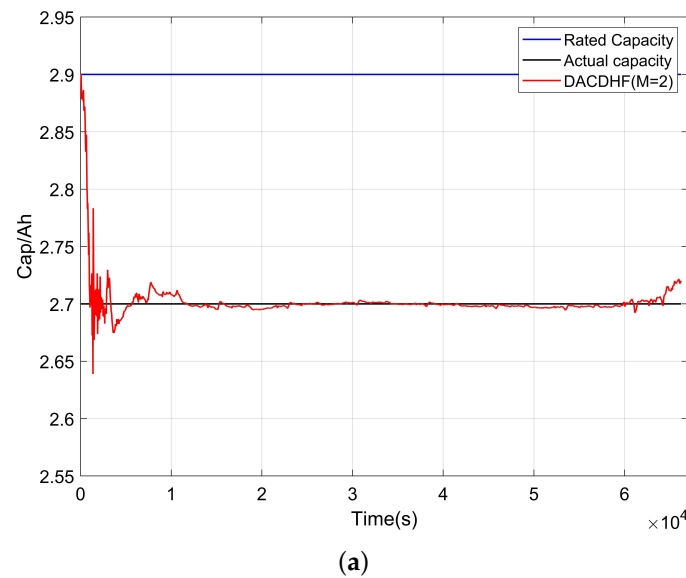


**Figure 11.** Cont.

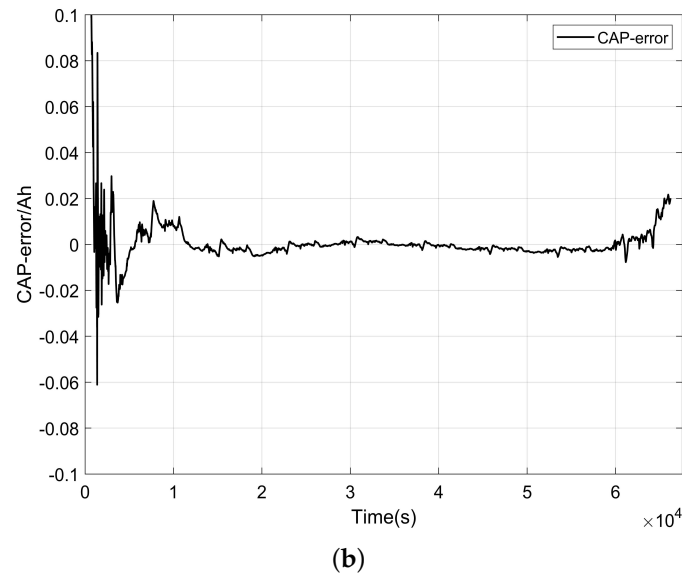


**Figure 11.** Capacity and error estimation results for HWFET operating conditions: (a) capacity estimation results; (b) capacity estimation error.

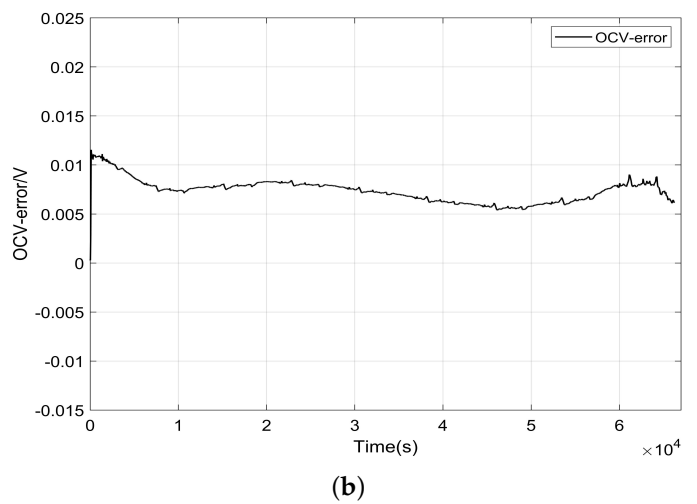
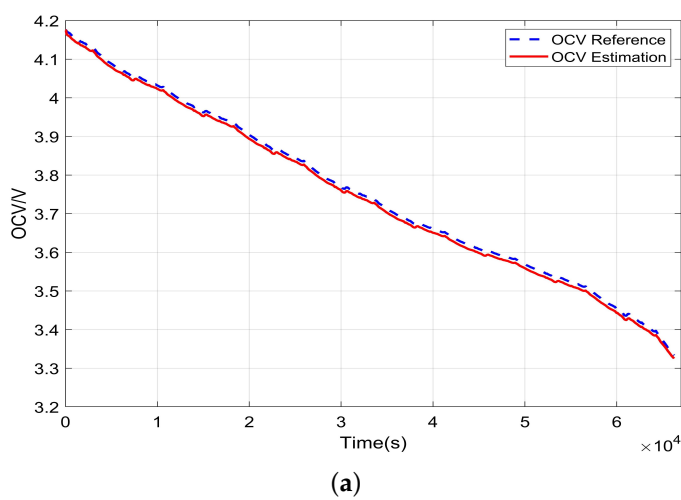


**Figure 12.** OCV and its error estimation results for HWFET conditions: (a) open-circuit voltage estimation results; (b) open-circuit voltage estimation error.

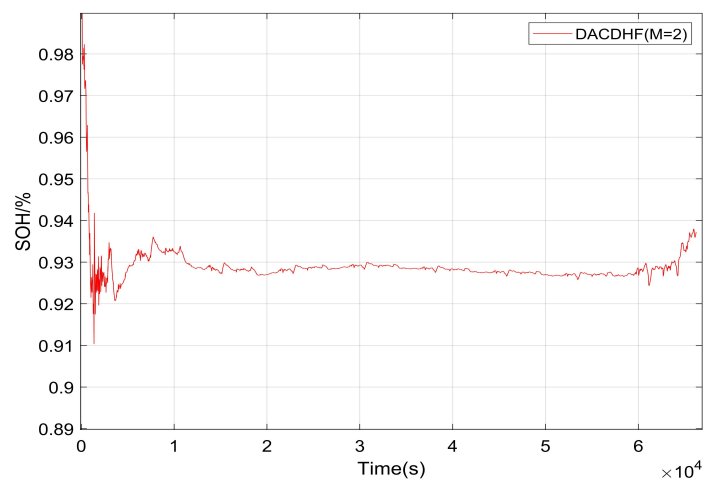


**Figure 13.** SOH estimation results for HWFET conditions.

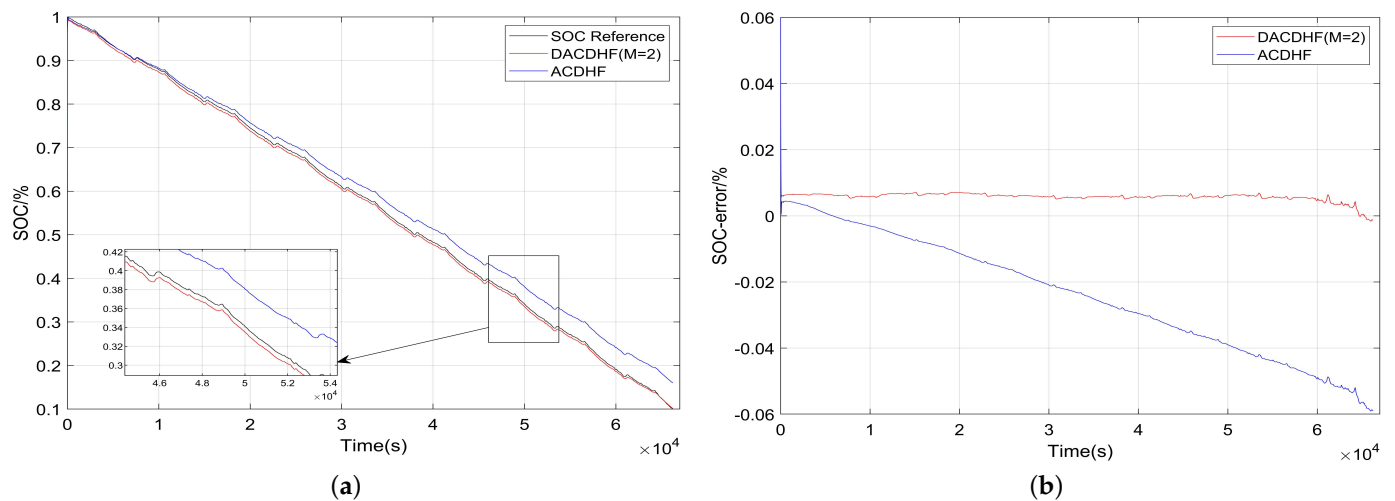


**Figure 14.** SOC estimation results and SOC error results for HWFET conditions: (a) SOC estimation results; (b) SOC error results.

## 5. Conclusions

In order to improve the estimation accuracy and convergence speed of SOC and SOH of lithium-ion batteries, a joint estimation algorithm based on DACDHF is proposed in this study. Firstly, based on the second-order RC equivalent circuit model, the IFFRLS algorithm is used for parameter identification. The model's output voltage accurately tracks the battery's actual voltage, with the error diminishing as the number of internal loops increases. Secondly, the capacity is selected as the SOH characteristic quantity. Considering the close relationship between OCV and capacity, and the interaction between SOC and SOH, the battery capacity estimation model and SOC estimation model are established, respectively. In addition, the DACDHF algorithm improves the error covariance matrix in the measurement update stage of the CDKF algorithm, and the Sage–Husa adaptive algorithm is introduced to update the measurement noise covariance matrix  $R$  so as to realize the joint estimation of SOC and SOH. Finally, experiments under UDDS and HWFET conditions are conducted with varied capacities and SOC initial values. The experimental results show that the convergence time of the capacity estimation is less than 8 min for both dynamic working conditions, the SOC estimation errors are 0.5% and 0.63%, and the SOH maximum estimation errors are 0.73% and 0.86%. The findings demonstrate that the proposed algorithm achieves superior estimation accuracy, faster convergence speed, and enhanced robustness.

**Author Contributions:** Conceptualization, B.S. and Z.W.; methodology, Y.W.; validation, B.S., J.W. and B.Y.; formal analysis, B.S. and Z.W.; investigation, B.S. and J.W.; resources, B.S. and B.Y.; data curation, B.S. and J.W.; writing—original draft preparation, B.S. and J.W.; writing—review and editing, J.W. and Y.W.; visualization, J.W. and Y.W.; supervision, B.S. and Z.W.; project administration, Z.W. and B.Y.; funding acquisition, B.S. and Y.W. All authors have read and agreed to the published version of the manuscript.

**Funding:** Supported by Open Fund of Jiangsu Engineering Technology Research Center for Energy Storage Conversion and Application (China Electric Power Research Institute), NY80-23-003. And supported by National Natural Science Foundation of China, 62373197, State estimation of target nodes in Multi-layer complex dynamic networks based on finite measurements.

**Data Availability Statement:** The data presented in this study are available on request from the corresponding author due to the confidentiality period of the project.

**Conflicts of Interest:** Authors Bingyu Sang and Bo Yang were employed by the company China Electric Power Research Institute. This study received funding from China Electric Power Research Institute. The remaining authors declare that the research was conducted in the absence of any commercial or financial relationships that could be construed as a potential conflict of interest.

## References

1. Lai, X.; Yuan, M.; Tang, X.; Yao, Y.; Weng, J.; Gao, F.; Ma, W.; Zheng, Y. Co-Estimation of State-of-Charge and State-of-Health for Lithium-Ion Batteries Considering Temperature and Ageing. *J. Energies* **2022**, *15*, 7416. [[CrossRef](#)]
2. Yihuan, L.; Kang, L.; James, Y.U. Estimation Approaches for States of Charge and Health of Lithium-ion Battery. *J. Power Gener. Technol.* **2021**, *42*, 537–546.
3. Ng, K.S.; Moo, C.S.; Chen, Y.P.; Hsieh, Y.C. Enhanced coulomb counting method for estimating state-of-charge and state-of-health of lithium-ion batteries. *J. Appl. Energy* **2009**, *86*, 1506–1511. [[CrossRef](#)]
4. Pei, L.; Lu, R.; Zhu, C. Relaxation model of the open-circuit voltage for state-of-charge estimation in lithium-ion batteries. *J. IET Electr. Syst. Transp.* **2013**, *3*, 112–117. [[CrossRef](#)]
5. Jiao, M.; Wang, D.; Qiu, J. A GRU-RNN based momentum optimized algorithm for SOC estimation. *J. Power Sources* **2020**, *459*, 228051. [[CrossRef](#)]
6. How, D.N.; Hannan, M.A.; Lipu, M.S.H.; Sahari, K.S.; Ker, P.J.; Muttaqi, K.M. State-of-charge estimation of Li-ion battery in electric vehicles: A deep neural network approach. *J. IEEE Trans. Ind. Appl.* **2020**, *56*, 5565–5574. [[CrossRef](#)]
7. Xiao, F.; Li, C.; Fan, Y.; Yang, G.; Tang, X. State of charge estimation for lithium-ion battery based on Gaussian process regression with deep recurrent kernel. *J. Int. J. Electr. Power Energy Syst.* **2021**, *124*, 106369. [[CrossRef](#)]
8. Wang, W.; Fu, R. Stability Analysis of EKF-Based SOC Observer for Lithium-Ion Battery. *Energies* **2023**, *16*, 5946. [[CrossRef](#)]
9. Zhang, X.; Wang, Y.; Xia, J.; Zhang, Y. Estimation of the SOC of lithium batteries based on an improved CDKF algorithm. *J. Energy Storage Sci. Technol.* **2021**, *10*, 1454–1462.
10. Xiong, R.; Yu, Q.; Lin, C. A novel method to obtain the open circuit voltage for the state of charge of lithium-ion batteries in electric vehicles by using H infinity filter. *Appl. Energy* **2017**, *207*, 346–353. [[CrossRef](#)]
11. Zhang, X.; Duan, L.; Gong, Q.; Wang, Y.; Song, H. State of charge estimation for lithium-ion battery based on adaptive extended Kalman filter with improved residual covariance matrix estimator. *J. Power Sources* **2024**, *589*, 233758. [[CrossRef](#)]
12. Xiang, L.; Cai, L.; Dai, N.; Gao, L.; Lei, G.; Li, J.; Deng, M. State of Charge Estimation of Lithium-Ion Batteries Based on an Improved Sage-Husa Extended Kalman Filter Algorithm. *World Electr. Veh. J.* **2022**, *13*, 220. [[CrossRef](#)]
13. Zhao, J.; Tian, L.; Cheng, L. Review on State Estimation and Remaining Useful Life Prediction Methods for Lithium-ion Battery. *Power Gener. Technol.* **2023**, *44*, 5014. [[CrossRef](#)]
14. Shen, P.; Ouyang, M.; Lu, L.; Li, J.; Feng, X. The Co-estimation of State of Charge, State of Health, and State of Function for Lithium-Ion Batteries in Electric Vehicles. *IEEE Trans. Veh. Technol.* **2018**, *67*, 92–103. [[CrossRef](#)]
15. Zou, Y.; Hu, X.; Ma, H.; Li, S.E. Combined State of Charge and State of Health estimation over lithium-ion battery cell cycle lifespan for electric vehicles. *J. Power Sources* **2015**, *273*, 793–803. [[CrossRef](#)]
16. Hu, P.; Tang, W.F.; Li, C.H.; Mak, S.L.; Li, C.Y.; Lee, C.C. Joint State of Charge (SOC) and State of Health (SOH) Estimation for Lithium-Ion Batteries Packs of Electric Vehicles Based on NSSR-LSTM Neural Network. *J. Energies* **2023**, *16*, 5313. [[CrossRef](#)]
17. Cheng, Z.; Yang, L.; Sun, X.M. State of Charge and State of Health Estimation of Li-ion Batteries Based on Adaptive Square-root Unscented Kalman Filters. *J. Proc. CSEE* **2018**, *38*, 2384–2393+2548.
18. Yiqi, L.; Wanjun, L.; Qian, L.; Yichao, G.; Ming, D. Joint State Estimation of Lithium-Ion Battery Based on Dual Adaptive Extended Particle Filter. *J. Trans. China Electrotech. Soc.* **2024**, *39*, 607–616.
19. Ruoqi, W.; Xiaojia, W.; Qi, Y. Joint Estimation of Lithium Battery SOC/SOH Based on Double Adaptive Untracked Kalman Filtering Algorithm. *Mach. Des. Manuf.* **2023**, *1*, 1–4.
20. Yu, Q.; Xiong, R.; Yang, R.; Pecht, M.G. Online capacity estimation for lithium-ion batteries through joint estimation method. *J. Appl. Energy* **2019**, *255*, 113817. [[CrossRef](#)]
21. Tan, Z.; Peng, T.; Dai, N.; Cai, L.; Wei, J.; Chen, H. Joint estimation of lithium battery SOC and SOH based on improved DAEKF. *J. Chongqing Univ. Posts Telecommun. (Nat. Sci. Ed.)* **2023**, *35*, 760–766.
22. Ren, B.; Xie, C.; Sun, X.; Zhang, Q.; Yan, D. Parameters Identification of Lithium-ion Battery Based on the Improved Forgetting Factor Recursive Least Squares Algorithm. *J. IET Power Electron.* **2020**, *3*, 2531–2537. [[CrossRef](#)]
23. Hu, C.; Youn, B.D.; Chung, J. A multiscale framework with extended Kalman filter for lithium-ion battery SOC and capacity estimation. *Appl. Energy* **2012**, *92*, 694–704. [[CrossRef](#)]

**Disclaimer/Publisher's Note:** The statements, opinions and data contained in all publications are solely those of the individual author(s) and contributor(s) and not of MDPI and/or the editor(s). MDPI and/or the editor(s) disclaim responsibility for any injury to people or property resulting from any ideas, methods, instructions or products referred to in the content.